PNAS RESEARCH ARTICLE | IMMUNOLOGY AND INFLAMMATION

Interferon-induced activation of dendritic cells and monocytes by yellow fever vaccination correlates with early antibody responses

Elena Winheim[a], Antonio Santos-Peral[b], Tamara Ehm[a], Linus Rinke[a], Sandra Riemer[a], Magdalena Zaucha[b,c], Sebastian Goresch[b], Lisa Lehmann[b], Katharina Eisenächer[a], Michael Pritsch[d], Giovanna Barba-Spaeth[e], Tobias Straub[f], Simon Rothenfusser[b,c], and Anne B. Krug[a,1]

Affiliations are included on p. 11.

Edited by Marco Colonna, Washington University in St. Louis School of Medicine, St. Louis, MO; received October 29, 2024; accepted March 18, 2025

Yellow fever vaccination provides long-lasting protection and is a unique model for studying the immune response to an acute RNA virus infection in humans. To elucidate the early innate immune events preceding the rapid generation of protective immunity, we performed transcriptome analysis of human blood dendritic cell (DC) and monocyte subpopulations before and 3, 7, 14, and 28 d after vaccination. We detected temporary upregulation of IFN-stimulated genes (ISG) in all DC and monocyte subsets on days 3 and 7 after vaccination as well as cell type–specific responses and response kinetics. Single-cell RNA sequencing revealed rapid appearance of activated DC and monocyte clusters dominated by ISGs, inflammatory chemokines, and genes involved in antigen processing and presentation. This was confirmed by flow cytometric analysis in a large cohort of vaccinees. We identified SIGLEC1/CD169 upregulation as a sensitive indicator of the transient IFN-induced activation state elicited in DCs and monocytes by YF17D vaccination correlating with early protective IgM antibody responses.

dendritic cells | yellow fever virus | vaccination | monocytes | interferon

Significance

The yellow fever vaccine is one of the most successful vaccines available. After a single dose, it induces long-lasting protective immunity against yellow fever, a severe disease caused by the yellow fever virus which is transmitted by mosquitoes. It is not clear why this live vaccine is so exceptionally efficient. Antigen-presenting cells (APCs) are crucial for the induction of immunity against viral infection. We therefore investigated the early response of APC subpopulations in the blood of healthy vaccinees and found that a specific activation state of APCs induced by interferons was associated with the early production of protective antibodies.

Acute viral infections caused by flaviviruses such as yellow fever (YF), dengue, and West Nile virus represent a major global health threat. The attenuated YF vaccine virus 17D-204 (YF17D) is one of the most successful live-attenuated vaccines available and provides long-lasting immune protection against yellow fever after a single dose (1–4). Therefore, this vaccine can be used as an excellent model to study the immunological characteristics of a highly efficient and long-lasting protective immune response to an acute self-limited RNA virus infection.

The response to YF17D is marked by a systemic innate immune response involving the induction of and response to type I interferons, and inflammasome activation in peripheral blood mononuclear cells within the first week after vaccination (5–7). YF17D vaccination in rare incidents can cause life-threatening viscerotropic or neurotropic disease. In a recent study of eight patients with severe vaccine-associated disease, *IFNAR1* and *IFNAR2* deficiency as well as neutralizing autoantibodies against type I IFNs accounted for more than half of the cases, demonstrating the importance of the type I Interferon response in controlling YF17D replication and inducing protective immune responses (8, 9). Characteristically a transient activation of circulating dendritic cells (DCs) and monocytes within the first week after vaccination (10) is followed by the activation and expansion of specific $CD4^+$ and $CD8^+$ T cells with a peak between 11 and 14 d after vaccination (11–13). A strong humoral immune response with neutralizing antibodies initially dominated by IgM is detected within 2 wk and persists in the majority of vaccinated patients (4, 14, 15). Data obtained in the mouse model suggest that the protective immune response to YF17D is mainly mediated by humoral immunity and $CD4^+$ T cell responses (16), but cytotoxic $CD8^+$ T cells are probably also relevant for long-term protection (17). Systems vaccinology approaches using the transcriptome of whole PBMC defined genes and gene modules that may predict the adaptive immune response to YF17D and other vaccines. For example, expression of genes encoding molecules involved in the stress-response pathway such as *EIF2AK4* and B cell genes such as *TNFRSF17* were found to be predictive of the $CD8^+$ T cell and antibody responses to YF17D respectively (7). Subsequently "blood transcriptional modules" were identified that correlated with antibody responses across several vaccines including YF17D (18, 19). However, a comprehensive analysis of the responses of the different human DC and monocyte subpopulations to YF17D vaccination and their association with parameters of adaptive immunity is lacking until now.

Preprint server: https://www.biorxiv.org/content/10.1101/2024.07.31.606034v1 under a CC-BY-ND 4.0 International license.

Author contributions: E.W., K.E., T.S., S.R., and A.B.K. designed research; E.W., A.S.-P., L.R., M.Z., S.G., L.L., and M.P. performed research; G.B.-S. contributed new reagents/analytic tools; E.W., A.S.-P., T.E., L.R., S.R., M.Z., L.L., and T.S. analyzed data; S.R. and M.P. initiated the cohort; M.P. performed vaccinations served as clinical study investigator, acquired funding, and supervised; G.B.-S. acquired funding; S.R. and A.B.K. interpreted data, acquired funding, supervised; and E.W. and A.B.K. wrote the paper.

The authors declare no competing interest.

This article is a PNAS Direct Submission.

[1]To whom correspondence may be addressed. Email: anne.krug@med.uni-muenchen.de.

This article contains supporting information online at https://www.pnas.org/lookup/suppl/doi:10.1073/pnas.2422236122/-/DCSupplemental.

Published May 7, 2025.

Circulating monocytes rapidly respond to pathogens and pathogen-derived molecules by producing inflammatory mediators including cytokines and chemokines. Human monocytes comprise three subpopulations: $CD14^+$ classical monocytes, $CD14^+$ $CD16^+$ intermediate monocytes, and $CD14^{lo}$ $CD16^+$ nonclassical patrolling monocytes. An increased frequency of proinflammatory $CD14^+$ $CD16^+$ intermediate monocytes has been observed in patients with bacterial sepsis, dengue fever, Zika virus, and SARS-CoV2 infection (10, 20–22) and also in response to YF vaccination (10, 23). DCs are professional antigen-presenting cells (APCs) and essential for recognizing viruses and presenting viral antigens to T cells for induction of efficient adaptive immunity. In the human peripheral blood, we distinguish three types of conventional DCs (cDC1, cDC2, and DC3), plasmacytoid DCs (pDC), and transitional DCs (tDCs) (24–26). While cDC1 preferentially promote cytotoxic T cell and Th1 responses, cDC2 are important for T helper (Th)2, Th17, and T follicular helper responses. DC3 which are phenotypically similar to cDC2 but also exhibit monocytic traits were shown to be proinflammatory and promote Th1 and Th17 responses and $CD8^+$ tissue-resident memory T cells (27–29). $CD14^+$ DC3 were described as an inflammatory DC subset that increases in frequency in the blood during flares of systemic lupus erythematosus (SLE) (29) and in COVID-19 patients correlating with disease severity (30). pDCs produce large amounts of type I IFNs in response to viral stimulation. tDCs, also called pre-DCs or Axl+ Siglec 6 + (AS)-DCs (24, 26, 31) can give rise to cDCs with cDC2 phenotype suggesting they are cDC2 precursors. At the same time, tDC actively participate in immune responses suggesting they have additional functions beyond their role as precursors (30, 32).

We hypothesized that functionally distinct DC and monocyte subpopulations show common as well as unique responses to YF17D vaccination and we sought to define cell type-specific activation states associated with effective and long-lasting adaptive immune responses in a vaccination cohort of naïve healthy adults.

Results

YF17D Immunization Induces a Common Core Signature of IFN-Stimulated Genes in All APC Subsets and Cell Type–Specific Responses. To characterize the response of circulating APC subpopulations to YF17D vaccination, bulk RNA sequencing was performed on sorted DC and monocyte subsets, B cells as well as total PBMCs, before and on days 3, 7, 14, and 28 after vaccination in four healthy donors, two males and two females between 23 and 27 y of age (Fig. 1*A*). Principal component analysis (PCA) of the cell subset transcriptomes showed positioning of the samples governed by cell type. B cells and PBMCs were separated from DCs and monocytes in PC2 (Fig. 1*B*). Along PC1, pDC samples clustered together, followed by tDCs, cDC2, DC3, and then classical (mo1), intermediate (mo^{int}), and nonclassical monocytes (mo2). Time point after vaccination contributed little to the overall variance. Thus, circulating subsets of DCs and monocytes largely maintain their transcriptional identity after vaccination.

Gene signatures were extracted that allow distinction of DC subpopulations after acute viral stimulation. Cell type–defining genes preserved after vaccination included *CADM1*, *CLEC9A,* and *XCR1* for cDC1; *CD1C*, *GRIP1,* and *CD1E* for cDC2; *VSIG4*, *RNASE1,* and *DTNA* for *DC3*; *PLEKHD1*, *SMIM5,* and *VASH2* in pDCs; and *AXL*, *SIGLEC6,* and *ADAM33* in tDCs (*SI Appendix*, Fig. S1 and Dataset S1). While some populations like cDC1, pDCs, and tDCs showed clearly distinct gene expression profiles, cDC2, DC3, and monocytes gene signatures were overlapping, confirming the similarity of these populations seen in the PCA. DC3 characteristically expressed genes found in both monocytes (e.g., *F13A*) and in cDC2 (e.g., *CD1C*).

The greatest variance in gene expression was explained by cell type, but comparison of individual time points after vaccination to baseline within each population revealed time-dependent transcriptomic changes (Fig. 1*C* and Dataset S1). The highest average numbers of significantly up- and downregulated genes (differentially expressed genes, DEGs) were found on day 7 after vaccination in most cell types, indicating the peak of the systemic innate immune response. Both mo1 and DC3 showed a higher number of DEGs compared to the other populations, while mo^{int} were the least responsive cell type. In mo1 and pDCs, changes in transcriptome were still observed 28 d after vaccination, while gene expression in the other populations returned to baseline or showed only few DEGs at that time point.

By hierarchical clustering of genes showing significant changes in expression over time, we identified distinct temporal patterns (Fig. 1*D* and Dataset S2). Each cell population exhibited multiple clusters with different dynamics. In the majority of DC and monocyte subpopulations (cDC2, DC3, mo1, mo2, and pDCs), the largest clusters (Fig. 1*D*, indicated in bold) were those with a peak on day 7 and/or day 3 after vaccination confirming the results of the DEG analysis shown in Fig. 1*C*. Notably, each cell population, except for PBMCs, had a cluster with peak gene expression on day 7 postvaccination (Fig. 1*D*, red). Overrepresentation analysis using MSigDB Hallmark and C2 canonical pathways showed significant enrichment for the Reactome pathway "Interferon gamma signaling" and "Interferon alpha response" or "Interferon alpha/beta signaling" in these predominant clusters across all populations (Dataset S2).

In cDC1 and tDCs, the largest clusters showed the highest level of gene expression before vaccination followed by a decrease on day 3 and fluctuation at later time points. In cDC1 cluster 1, genes from the Hallmark pathways "TNFα signaling via NF-κB" and "P53 pathway" were overrepresented. Conversely, tDCs cluster 1 showed no significant pathway enrichment but contained genes such as *RAD1* and *ZBTB40* involved in cell cycle checkpoints and transcriptional regulation. In PBMCs, B cells, and mo^{int} the largest clusters encompassed genes with increased expression on day 28 compared to the other time points: in B cells, cluster 3 with this dynamic was enriched for genes from Reactome pathways "Cellular response to chemical stress", "Fatty acid metabolism," and KEGG pathway "Oxidative phosphorylation." Within the PBMC cluster 1, we found genes such as *IFNLR1*, *GZMB,* and *VEGFB* while in mo^{int} cluster 2 we found genes such as *HMGB1*. Temporal gene clusters with a similar upregulation at the later time points were also found in the other subsets most prominently in mo1 (cluster 5) and pDCs (cluster 5) consistent with the higher number of DEGs observed between d28 and d0 in these subsets. Cluster 5 in mo1 was enriched for ISGs, Hallmark "E2F targets", "Adipogenesis" and Fatty Acid Metabolism. We also observed biphasic clusters with peaks on day 3 and day 14. These were enriched for Reactome Interferon alpha/beta signaling and Interferon gamma signaling in mo2 and Hallmark Fatty acid metabolism and Adipogenesis in mo1. Thus, common and diverse dynamics of gene expression were observed in the different populations highlighting the complex and coordinated early immune response to YF17D vaccination.

Comparing the DEGs of day 7 vs. baseline between the different APC subsets we identified a group of commonly upregulated genes (Fig. 1*E*). This shared response gene signature consisted of 12 interferon-stimulated genes (ISGs): *IFITM1*, *IFIT3*, *IFI6*, *OASL*, *SP110* (also known as *IFI41* or *IFI75*), *IFI44L*, *ISG15*, *RSAD2*, *OASL*, *XAF*, *OAS2*, and *EIF2AK2*. Depending on the

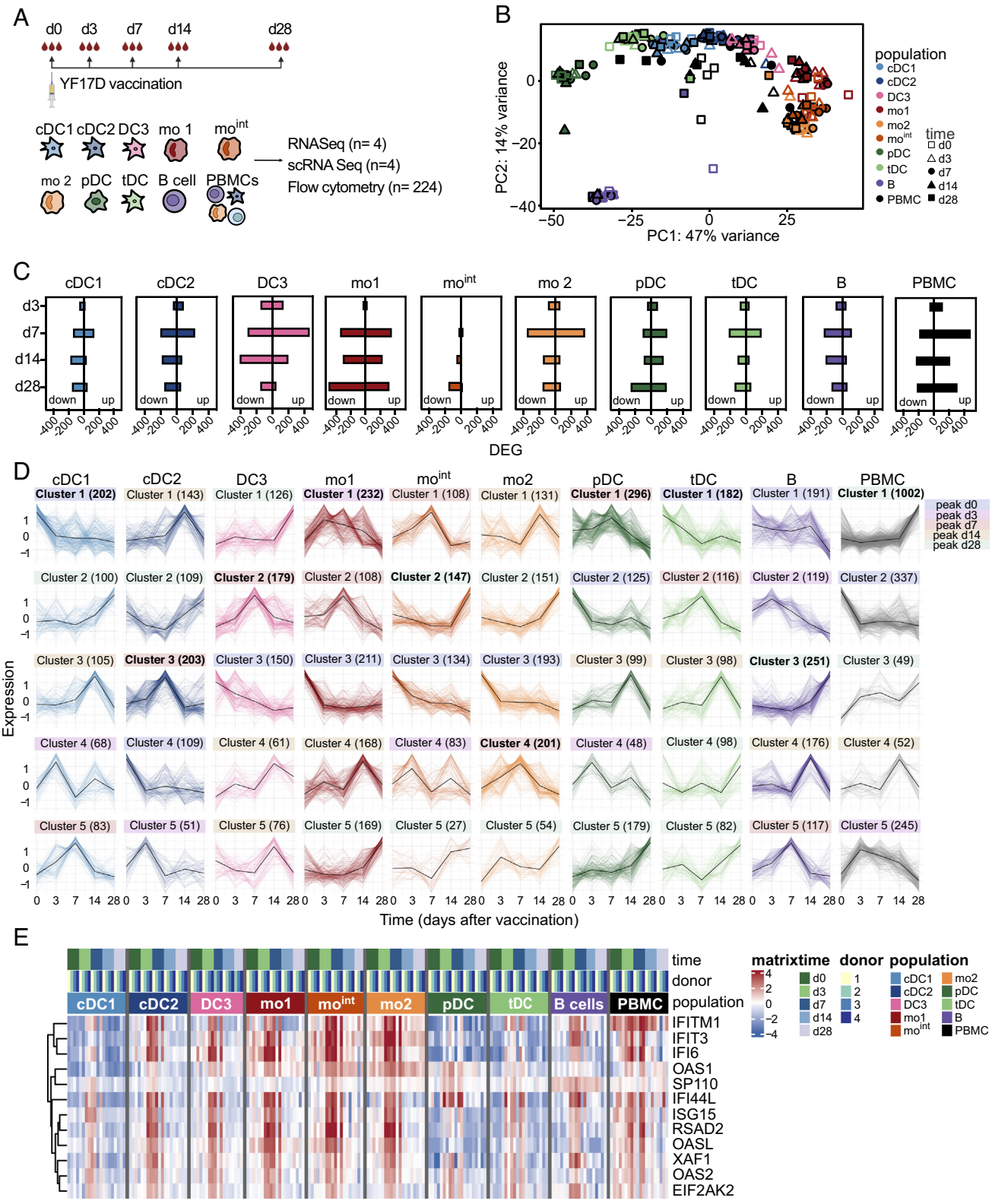

Fig. 1. YF17D vaccination induces common and distinct time-dependent transcriptome changes in blood APC subpopulations. (*A*) Experimental design of the study. (*B*) PCA of VST-transformed bulk RNA-seq data after prefiltering. Sorted populations are indicated by colors and the symbols indicate the time after vaccination. (*C*) DESeq2 was used to find the significantly up- and downregulated genes (adjusted $P < 0.05$, Bonferroni corrected) of each population and each time point after YF17D vaccination compared to day 0. The number of up- and downregulated DEGs are shown and the colors indicate the populations. (*D*) Expressed genes (log counts per million ≥ 0.5) with significant changes in expression between time points (ANOVA, $P < 0.05$) were clustered according to their similar dynamic of expression over time for each population. Colored lines connect the average expression of each gene at the indicated time points (z-score scaled per row). Line colors refer to the cell populations. Clusters are numbered in random order. Clusters in bold have the highest gene number compared to other clusters within the population. Numbers in brackets indicate the number of genes in each cluster. Cluster headings are highlighted in colors indicating different dynamics with peak of gene expression on day 0 (blue), on day 3 (pink), on day 7 (red), on day 14 (orange), or on day 28 (green). (*E*) Heatmap showing hierarchically clustered DEG upregulated on day 7 vs. day 0 common to all APC subsets (cDC1, cDC2, DC3, mo1, mo^{int}, mo2, tDC, pDC, B, and PBMCs). Gene expression is indicated by the color (red: high expression, blue: low expression) for each donor and all DC and monocyte subpopulations, B cells, and PBMCs. Time points, vaccinees, and subpopulations indicated by colors above the heatmap. Four samples were excluded due to insufficient quality.

individual vaccinee, these genes were upregulated on day 3 and/or on day 7 and returned to baseline on day 14 after vaccination reflecting a regulated temporary ISG response. Thus, distinct populations of APCs showed common and distinct dynamics of gene expression and shared a core ISG response peaking on day 3 or 7 after yellow fever vaccination.

Gene set enrichment analysis (GSEA) comparing each time point with the baseline before vaccination in all APC populations using all expressed genes confirmed the common enrichment of ISGs on days 3 and 7 after vaccination (Fig. 2*A*). Reactome "Antigen processing and presentation" was enriched in all DC subsets, in mo^{int} and mo2 at all time points with peak on day 7 (Fig. 2*A* and *SI Appendix*, Fig. S2*A*). Gene sets involved in translational pathways, oxidative phosphorylation, and respiratory electron transport were underrepresented in mo1 on days 3, 7, and 14, in pDCs on day 14, and in cDC1 on day 3, but were enriched in cDC2, DC3, and tDCs at all time points and cDC1 at later time points indicating differences between cell types in the metabolic response and impact of the vaccination on ribosome biogenesis and translation (Fig. 2*A*).

We next compared DEGs (d7 vs. d0) between related APC populations (Fig. 2*B*). tDCs shared more response genes with cDC2 than with pDCs. Hallmark gene set "Interferon gamma response" was overrepresented uniquely in cDC2 when compared to pDCs and tDCs. DC3, mo1, and cDC2 had many overlapping peak response genes with overrepresentation of ISGs as expected. Response genes shared between DC3 and cDC2 were enriched for "antigen processing and cross-presentation," "proteasome," "signaling by Wnt," "MAPK family signaling cascades," "C-type lectin like receptors," and "Interleukin 1 family signaling" while response genes unique for mo1 were enriched in Hallmark "inflammatory response" and "TNF-α signaling via NFκB." This unique response in mo1 was also observed in comparison with mo^{int} and mo2. Unique among the monocyte subsets mo2 response genes showed overrepresentation of "Class I MHC mediated antigen processing and presentation." cDC1, cDC2, and DC3 shared many peak response genes. Besides ISG these were enriched for Reactome gene sets "Class I MHC mediated antigen processing and presentation" and "signaling by interleukins" highlighting their common antigen presentation function (Fig. 2*B* and Dataset S3).

Further analysis of cell type–specific response genes revealed for example upregulation in cDC1 of lysosomal associated membrane protein 3 (*LAMP3*) implicated in DC maturation and MHC class II presentation (33) and transient upregulation of chemokine expression, e.g., *CXCL10*, *CCL2,* and *CCL7* particularly in monocytes (*SI Appendix*, Fig. S2*B*). *DDX58*, encoding viral RNA sensor RIG-I, was also significantly upregulated in monocytes, and less so in cDC2 and DC3 suggesting that these cell types become more responsive to RIG-I ligands after vaccination (*SI Appendix*, Fig. S2*B*).

Thus, besides a common ISG-dominated response to YF17D we detected cell type–specific changes in gene expression suggesting distinct functional contributions of different DC and monocyte subpopulations.

Single-Cell RNA Seq Reveals Activated Cell Clusters Expressing ISGs and Inflammatory Genes on Days 3 and 7 After Vaccination. The expression of response genes in defined cell populations may be heterogeneous with several differentiation and activation states coexisting within the same subpopulation. To identify distinct activation states within APC subpopulations in an unbiased manner, we performed single-cell RNA sequencing (scRNA-seq) of the DC and monocyte fractions sorted from PBMCs of four donors (two males and two females) before and at day 3 and 7 after vaccination. Sorted DCs and monocytes of each donor were combined at a ratio of 4:1 to enrich DCs and increase the cell number for rare DC subsets. After removing doublets and

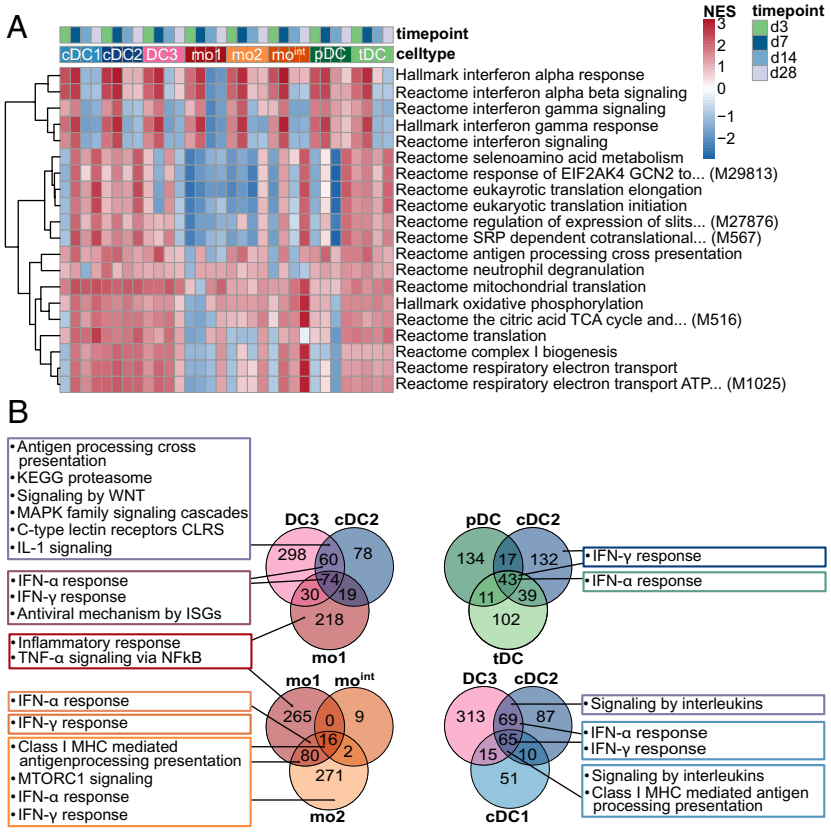

Fig. 2. Transcriptome response of circulating APC subsets to YF17D is dominated by ISGs. (*A*) Heatmap of unscaled normalized enrichment scores (NES) for selected pathways from Hallmark and Reactome across four time point comparisons against baseline. Displayed pathways include only those with NES greater than 2 in at least one comparison. GSEA was applied using the t-statistic of each comparison. Upper margin colors indicate populations and time points. The color scale bar represents NES values. (*B*) Venn diagrams showing the number of overlapping and distinct DEGs upregulated on d7 vs. d0 (*P*adj. < 0.05) in the indicated set of populations. Hallmark and Reactome pathways identified by overrepresentation analysis are shown for DEGs unique to one population or overlapping between populations for each Venn diagram.

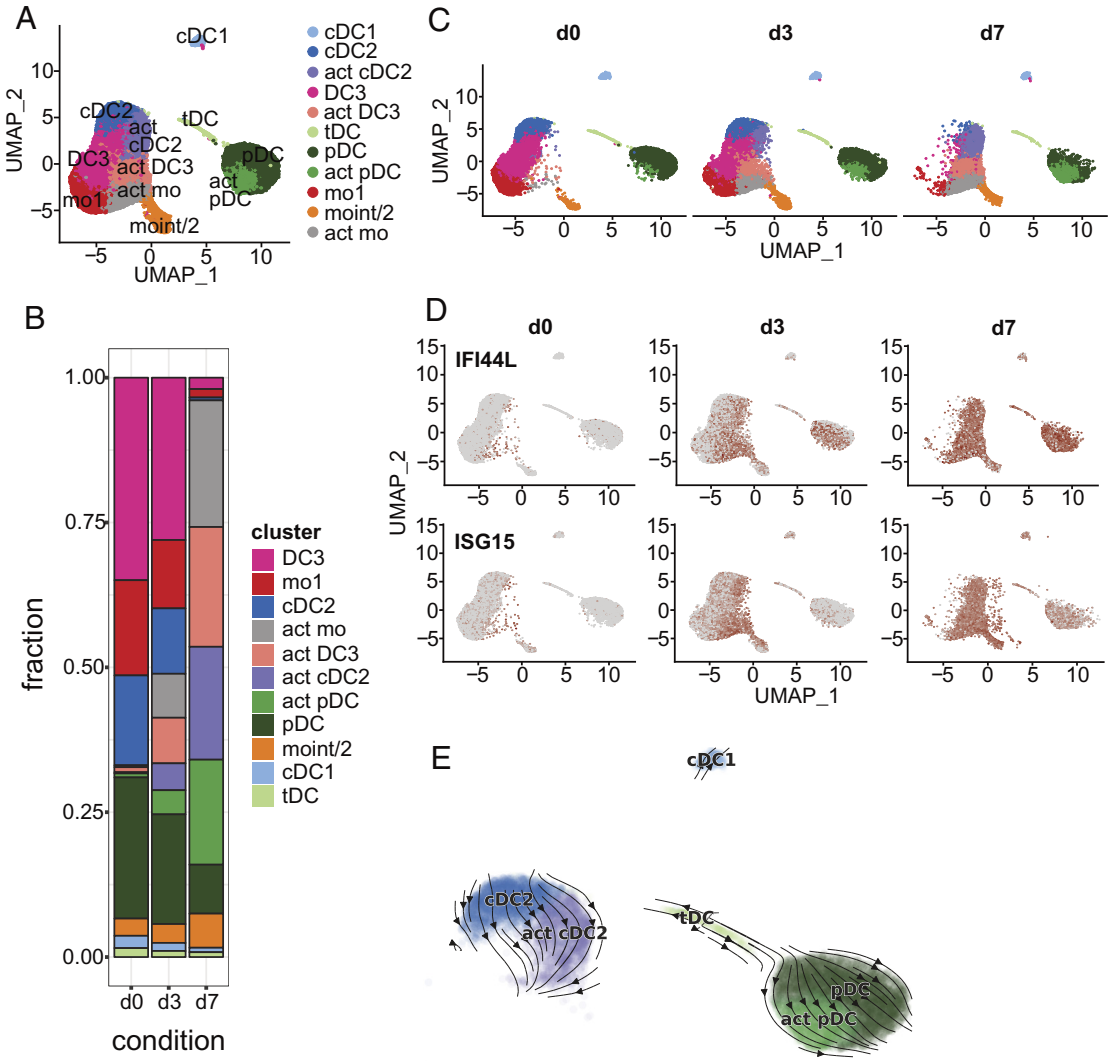

Fig. 3. scRNA-seq indicates collective acquisition of an activated cell state in blood DCs and monocytes early after vaccination. (*A*) UMAP visualization of concatenated scRNA-seq data with the annotated cell clusters (Louvain) indicated by colors. (*B*) Stacked bars show the frequency of the individual populations annotated before (d0) and at d3 and d7 after vaccination. (*C*) UMAP visualization of scRNA-seq data from different time points (before (d0) and at d3 and d7 after vaccination). (*D*) Color overlay showing expression of IFI44L and ISG15 as color overlay projected onto UMAP from *C*. Red = high expression, gray = low expression. (*E*) The RNA velocity vector field derived from scvelo analysis of cells identified as cDCs, pDCs, and tDCs (all donors and time points combined) was projected onto the UMAP with annotated cell clusters indicated by colors.

cells with high mitochondrial RNA (>7.5%) or low total RNA (<200 genes), we analyzed ~35,000 cells. Individual donors were integrated using harmony normalization. Unbiased clustering revealed 14 clusters, with clusters 3, 4, 6, and 7 found mostly on days 3 and 7 after vaccination (*SI Appendix*, Fig. S3 *A* and *B*). These clusters showed high expression of ISGs indicating an activated antiviral cell state (*SI Appendix*, Fig. S3*C*).

The individual clusters were annotated manually using known marker genes for DC and monocyte subpopulations derived from publications (26, 29) and our own bulk RNA gene signatures (*SI Appendix*, Fig. S3 *C* and *D*). After merging highly similar clusters, cDC1, cDC2, DC3, mo1, mo^{int}/mo2, tDC, and pDC populations as well as activated cDC2, activated DC3, activated pDC, and activated monocytes expressing ISGs exemplified by *IFI44L* and *ISG15* were identified (Fig. 3 *A* and *D*). The percentages of cells found in the activated DC and monocyte clusters greatly increased on days 3 and 7 (Fig. 3*B*). This ISG-driven response was most prominent in cDC2, DC3, and mo1 where on day 7, the activated clusters almost entirely replaced the clusters found on day 0 (Fig. 3*C*). In three donors, a partial shift toward more activated cells was already seen on day 3 after vaccination (*SI Appendix*, Fig. S4*A*). These results demonstrate that most cells responded to the vaccination in a concerted fashion especially cDCs and monocytes with full activation reached by day 7. *IFN-Typ I/III* transcripts were not detected above threshold in this dataset at any of the time points investigated (Fig. 4*C*) similar to the bulk RNA-seq results (*SI Appendix*, Fig. S2*C*). IFN-α2, IFN-β, IFN-γ, IFN-λ1, and -λ2 were measured in plasma samples from day 0, 3, 7, 14, and 28 in a subgroup of 22 vaccinees using a bead-based multiplex assay, but could not be detected in any of the samples.

Since tDCs were previously shown to differentiate into cells with a cDC2 phenotype in vitro (24) and in mice in vivo (32, 34), we inferred trajectories from RNA velocity analysis of the combined data of cDC and pDC subsets from all time points using the scVelo method. RNA velocity vectors were bidirectional pointing from tDCs toward cDC2 as well as pDCs (Fig. 3*E*). This was confirmed using two additional pseudotime ordering methods (diffusion pseudotime and Palantir, *SI Appendix*, Fig. S4 *B*–*D*). These results suggest that human tDCs are heterogeneous and contain cells with divergent trajectories toward pDCs and cDC2.

Pairwise comparison between the activated and nonactivated APC clusters confirmed upregulation of ISGs such as *IFI44L*,

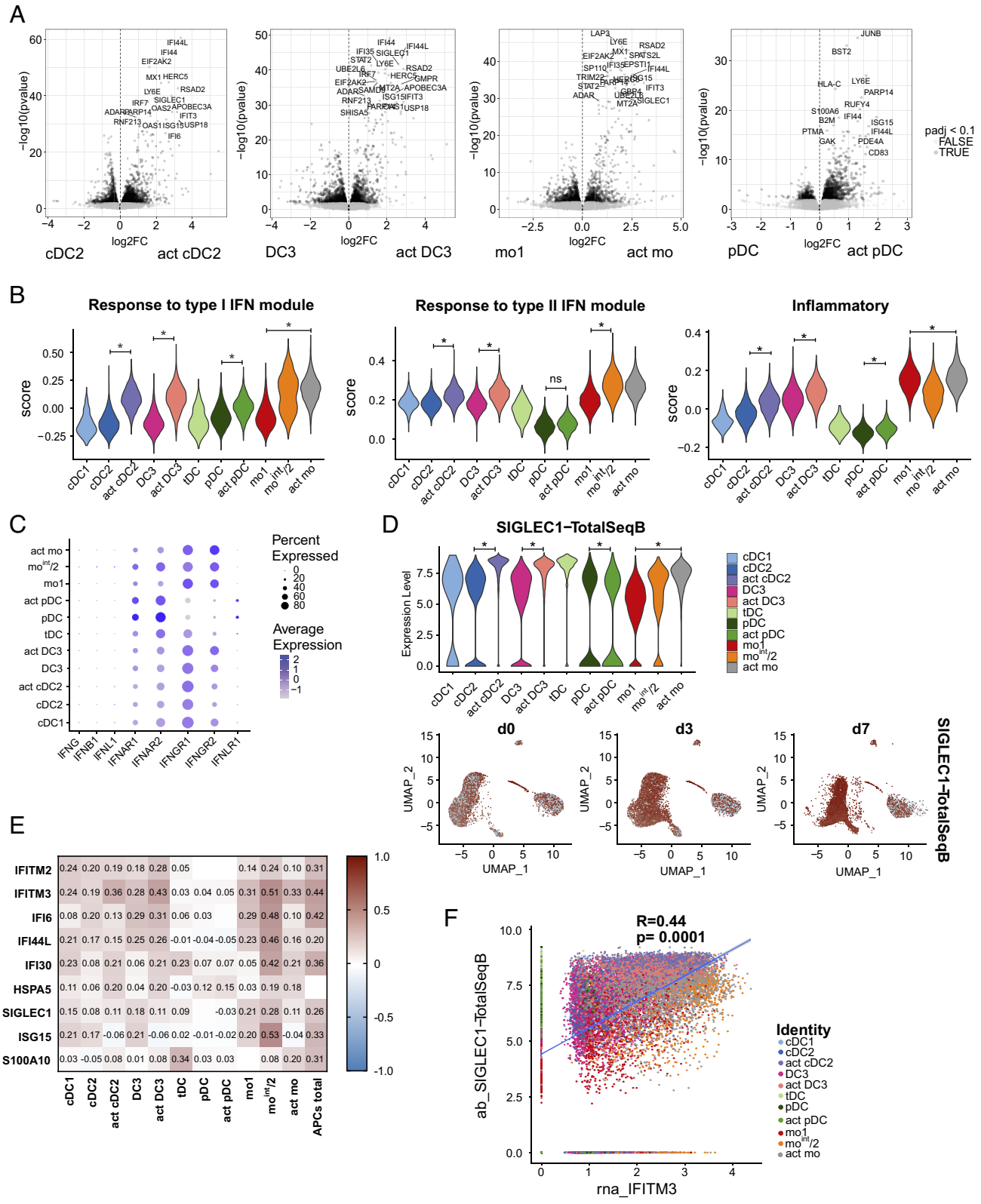

Fig. 4. SIGLEC1 expression on the cell surface marks the IFN-induced activation state in cDC2, DC3, and monocytes. (*A*) Volcano plots showing comparison of activated and nonactivated clusters of cDC2, DC3, mo1, and pDCs with annotation of significantly up-and downregulated genes (*P*-value < 0.1, log2 fold-change > 0.3). (*B*) Violin plots showing the indicated gene expression scores based on average counts of the module genes in each cell cluster. Significant difference of scores between activated and nonactivated cell clusters are indicated by asterisks (Wilcoxon test using the mean module scores of the individual donors, n = 4). (*C*) Dot plot showing the expression of all detected IFN and IFN receptor genes in the cell clusters. Color intensities indicate the average gene expression values and diameters indicate the percentages of cells expressing the genes within the cluster. (*D*) Violin plot showing surface expression of SIGLEC1 as measured using TotalSeqB antibody. UMAP showing surface expression of SIGLEC1 detected by TotalSeqB antibody as color overlay projected onto the separate UMAP before and on days 3 and 7 after vaccination. Red: high expression; gray: low expression. (*E*) Pearson correlation analysis of surface SIGLEC1 expression. Correlation coefficients (R values) are shown in the heatmap for selected genes highly correlating with SIGLEC1 gene expression in each population. (*F*) Scatter plot of IFITM3 RNA expression and SIGLEC1 expression of all cells with linear regression line. Colors indicate belonging of cells to a specific cell cluster. Pearson correlation coefficient R and *P*-values are indicated in the graph.

EIF2AK2, and *ISG15* in activated clusters of cDC2, DC3, monocytes, and pDCs (Fig. 4*A*). Relative expression scores derived from the type I IFN-induced gene module (35) were significantly higher in the activated clusters (Fig. 4*B*). The type II IFN-induced gene module scores were also significantly increased in the activated compared to the nonactivated cDC2 and DC3 clusters and in the mo^{int}/mo2 cluster compared to mo1 (Fig. 4*B*). This was not the case for the activated pDC cluster coinciding with a lower mRNA expression level of IFN-γ receptors *IFNGR1* and *IFNGR2* in pDCs compared to cDCs and monocytes (Fig. 4*C*). Relative expression scores of the hallmark inflammatory gene set also tended to be increased in the activated compared to the nonactivated cDC2 and DC3 clusters and were constitutively high in monocytes and low in pDCs and tDCs (Fig. 4*B*). For cDC1 and tDCs where a separate activation cluster was not detected, we found significant upregulation of multiple ISGs on days 3 and 7 after vaccination compared to baseline confirming the bulk RNA-seq results (*SI Appendix*, Fig. S4*E*).

Expression of SIGLEC1 encoding for the CD169 surface molecule, which was one of the genes highly upregulated in the activated cDC2, DC3, and mo1 clusters (Fig. 4*A*), was quantified on the protein level in the same experiment using TotalSeq B antibody labeling and sequencing. It was highly expressed in tDCs and in the activated cDC2, DC3, and mo1 clusters (Fig. 4*D*). Surface expression of SIGLEC1 protein correlated positively with mRNA expression of different ISGs such as *IFITM2*, *IFITM3*, *IFI6*, *IFI30,* and *ISG15* within all cells analyzed together and in each individual cluster except for tDCs and pDCs (Fig. 4 *E* and *F*). Therefore, surface expression of SIGLEC1 is a sensitive marker for the early response to IFNs and marks the temporary activated state of circulating cDCs and monocytes after YF17D vaccination.

Upregulation of SIGLEC1 Coincides with Upregulation of Costimulatory Molecules and Activation Markers on the Surface of cDCs and Monocytes. To further characterize the functional state of circulating DC and monocyte subsets before and after YF17D vaccination and investigate interindividual variation of this response, we analyzed the phenotype of DC and monocyte subsets in cryopreserved PBMC samples by multidimensional spectral flow cytometry in a larger number of vaccinees. To link phenotype and transcriptome results, SIGLEC1/CD169 was included as a marker in addition to costimulatory molecules and chemokine receptors. First, PBMC from all four time points were analyzed in a subgroup of 10 patients. We detected temporary upregulation of mean fluorescence intensities (MFI) for CD86, PD-L1, and SIGLEC1 on day 7 after vaccination in all populations except for tDCs and pDCs consistent with the transcriptomic data. SIGLEC1 was already upregulated on day 3 and further increased on day 7 (Fig. 5 *A* and *B*). Expression of AXL, another IFN-induced surface molecule, was induced on day 7 in all DC subsets and in mo1 (Fig. 5*A*). CD83 was upregulated in cDC2, DC3, and monocytes on day 7. CD40 was also upregulated in many subsets on day 7 except in cDC1 and DC3. HLA-DR was upregulated in monocytes but not in DCs. CXCR3 expression was induced whereas CCR2 expression was reduced on day 7 in mo1 and in pDCs, whereas CCR2 expression was induced in mo2 indicating differential regulation of chemokine receptor expression between cell types after the vaccination. Population frequencies were also significantly altered after vaccination, with a shift from mo1 to mo^{int} and mo2 on day 7 and a slight reduction of cDC1 and cDC2 subsets (significant for cDC1) on day 7 after vaccination (*SI Appendix*, Fig. S5*A*) confirming previous results obtained from freshly isolated PBMC (10).

We selected the time points day 0 and day 7 to perform the same analysis for a cohort of additional 214 vaccinees. Significant increases in the MFIs of CD86, CD83, and AXL were detected on day 7 in all DC and monocyte subsets except for tDCs (Fig. 5 *B* and *D*). Upregulation of SIGLEC1 was detected in all subsets, except tDCs and pDCs. CD40 was significantly upregulated in pDCs and monocytes, but not in cDCs. Downregulation of CCR2 was observed in all populations, except for mo2. HLA-DR was significantly upregulated in monocyte subsets but rather downregulated in cDC subsets (Fig. 5*D*).

To identify activation clusters that might be missed by manual gating analysis, unbiased FlowSOM clustering was performed on the HLA DR$^+$ Lin$^-$ viable cells containing the DC and monocyte fractions. The clusters were visualized in a UMAP and assigned to monocytes or DCs according to the presence or absence of CD88/CD89 expression (*SI Appendix*, Fig. S5 *B–D*). The DC and monocyte fractions were then each clustered separately. Clusters were annotated and similar clusters were fused (*SI Appendix*, Fig. S5*E*). Within the DC fraction, cDC1, cDC2, CD163$^-$ DC3, CD163$^+$ CD14$^+$ DC3, SIGLEC1$^+$ DC3, tDC, and pDC were identified (Fig. 6 *A* and *B*). Monocyte clusters were annotated as mo1 (CD163$^-$ SIGLEC1$^-$), SIGLEC1$^+$ mo1, CD163$^+$ SIGLEC1$^-$ mo1, CD163$^+$ SIGLEC1$^+$ mo1, mo^{int}, mo2 (Fig. 6 *C* and *D*). Within the DC compartment, cDC1 and cDC2 were reduced and pDCs slightly increased. In the monocytes, the frequency of mo^{int} was significantly increased as seen previously in the exploration cohort (Fig. 6*E*). The frequency of cells in the SIGLEC1$^+$ DC3 and monocyte clusters increased dramatically on day 7 and only few vaccinees had SIGLEC1$^+$ cells at baseline with frequencies below 25% (Fig. 6*E*). Thus, the upregulation of SIGLEC1 surface expression on day 7 after YF17D vaccination and the appearance of distinct SIGLEC1$^+$ DC and monocyte clusters reflecting an IFN-induced activation state could be validated in a large cohort. Although an increase in SIGLEC1 expression was seen in the great majority of vaccinees on day 7 after vaccination, this response was variable between individuals warranting further investigation as a predictor of vaccination outcome.

High SIGLEC1 Upregulation on cDCs and Monocytes Is Associated with High Protective Antibody Titers Early After YF17D Vaccination. Vaccination with YF17D induced high titers of neutralizing antibodies (dominated by IgM isotype) on days 14 and 28 after vaccination indicating protection against infection was reached in all vaccinees of our cohort with highly variable titers (15). We hypothesized that the IFN-induced activation of blood cDCs and monocytes indicated by upregulation of SIGLEC1 surface expression relates to the rapid generation of protective antibody and T cell responses characteristic for YF vaccination. To explore this, we categorized individuals based on high and low SIGLEC1 fold-change (d7 vs. d0) in cDC1, cDC2, DC3, mo1, and mo2 through unsupervised clustering (Fig. 7*A*). pDCs and tDCs were excluded from the analysis due to the absence of SIGLEC1 upregulation postvaccination. Interestingly, the extent of SIGLEC1 upregulation was consistent across the different APC populations suggesting a concerted action and association with vaccine responsiveness. Stratification of vaccinees into high and low SIGLEC1 upregulation, with the exclusion of intermediate levels, allows a focused examination of this signature's impact on subsequent vaccine responses, which exhibit high variability across individuals.

Vaccinees with high SIGLEC1 upregulation on day 7 showed significantly higher neutralizing antibody titers and virus-specific IgM titers early after vaccination (day 14) than vaccinees with low

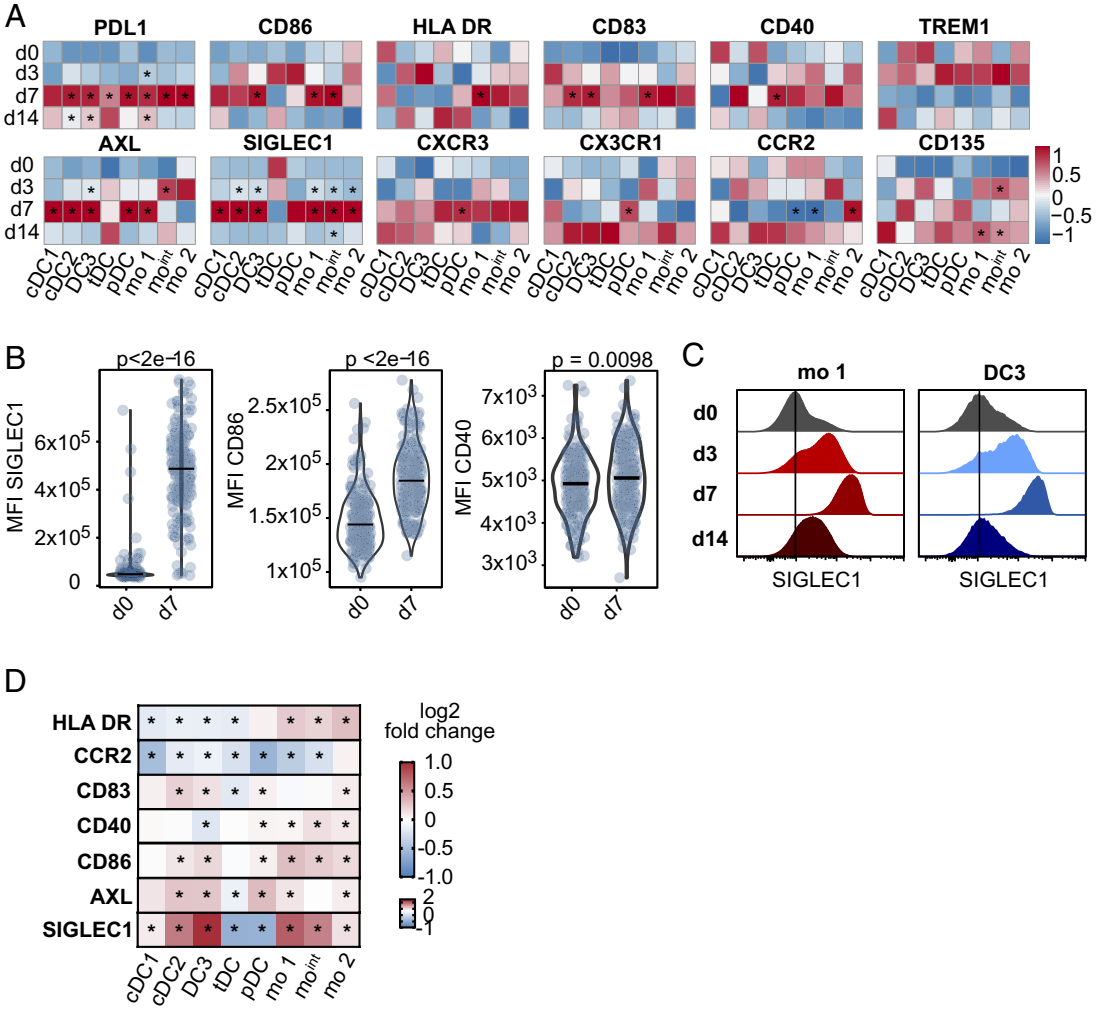

Fig. 5. Temporary upregulation of SIGLEC1 and costimulatory molecules characterizes the response of circulating APCs to YF17D in a large cohort of vaccinees. Phenotype of blood DC and monocytes subpopulations analyzed by flow cytometry. (*A*) Heatmap of the mean MFI values of indicated cell surface markers before vaccination (d0) and on days 3, 7, and 14 after vaccination (n = 10). The data are scaled for each column and significant differences to baseline are indicated by asterisks (*P < 0.05). Red: high expression, blue: low expression. (*B*) Violin plots showing the MFI of SIGLEC1, CD86, and CD40 on mo1 on days 0 and 7 after vaccination (n = 214). Measured values of individual study participants are indicated by blue-colored dots and P values shown in the graphs. (*C*) Histograms showing the SIGLEC1 expression level in mo1 and DC3 before vaccination (d0) and on days 3, 7, and 14 after vaccination (concatenated data of 10 donors). (*D*) Heatmap of the mean log2 fold change of the MFIs (d7 vs. d0) of the indicated surface markers (n = 214). Red: positive log2fc; blue: negative log2fc (−1 to 2 for SIGLEC1, −1 to 1 for all other markers). Significant differences to baseline are indicated by asterisks (*P < 0.05, Wilcoxon test, Bonferroni corrected).

SIGLEC1 upregulation (Fig. 7 *B* and *C*). Antigen-specific T cell responses and antibody responses on day 28 were not significantly altered between the subgroups (Fig. 7 *B* and *C*). Spearman rank correlation analyses confirmed the correlation of SIGLEC1 MFI on day 7 and fold change (d7 vs. d0) in DC3 and mo1 with early antibody titers. SIGLEC1 and CD86 expression correlated with each other and with day 7 plasma CXCL10 concentrations representing the systemic IFN-induced cytokine response. The frequency of mo^{int} on day 7 also positively correlated with plasma CXCL10 levels at the same time point. In sum, the temporary IFN-induced activation of circulating APCs detected by SIGLEC1 upregulation on day 7 after YF17D vaccination is associated with the early protective antibody response.

Discussion

Our study provides a comprehensive analysis of the temporal dynamics of gene expression in individual blood DC and monocyte subpopulations following YF17D vaccination in humans. We observed a transient ISG response within the first week after vaccination as the predominant feature in all subsets and defined a common set of significantly upregulated ISGs known to play a crucial role in the antiviral immune responses. Specifically, *IFI44L*, *OAS2*, *OAS3*, *IFIT2*, *IFIT3*, and *RSAD2* have been shown to impede viruses by disrupting viral replication and translation (36–40). Additionally, members of the IFN-inducible transmembrane family, such as *IFITM1* and *IFITM3*, obstruct viral entry and hinder early stages of the life cycle of various viruses (41). Consequently, this robust ISG signature reflects a systemic antiviral state within the circulating DC and monocyte compartment after YF17D vaccination which contrasts with the downregulation of ISGs that is seen in severe Dengue and Zika virus infections (42, 43). In the context of YF17D vaccination, several studies have identified the importance of a functional type I IFN response to control replication and pathogenicity of the vaccine virus. Patients with IFNAR1 and IFNAR2 deficiency or with autoantibodies against multiple type I interferons can present with life-threatening complications after vaccination (8, 9). Therefore, the antiviral state caused by upregulation of these ISGs seems to be highly relevant for controlling YF17D and ensuring the safety of this live vaccine. This is supported by the kinetic of viremia which is seen in a variable proportion of vaccinees between day 2 and day 9, but not thereafter (44–46).

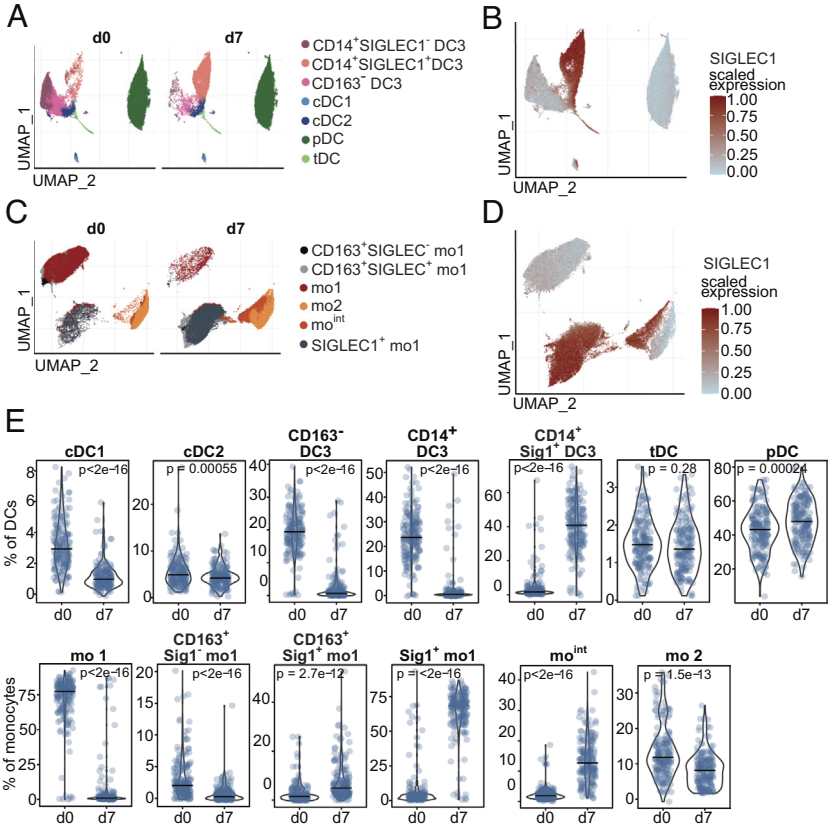

Fig. 6. Unbiased clustering of flow cytometric data confirms generation of SIGLEC1-positive DC3 and monocyte clusters with interindividual variability. FlowSOM clustering was performed on the HLA-DR$^+$ Lin$^-$ living cells containing both the DC and monocyte fractions. The clusters were visualized in a UMAP and assigned to monocytes or DCs according to the presence or absence of CD88/CD89 expression. Reclustering of DC and monocyte fractions was performed using FlowSOM. After annotating and fusing similar clusters, the data were depicted in a UMAP with annotated clusters shown as colored overlay. (*A*) Annotated DC clusters on d0 and d7 after vaccination. (*B*) SIGLEC1 scaled expression indicated by red-brown color overlayed on the UMAP embeddings of DCs. (*C*) Annotated monocyte clusters on d0 and d7 after vaccination. (*D*) SIGLEC1 scaled expression indicated by red-brown color overlayed on the UMAP embeddings of monocytes. (*E*) Violin plots show DC and monocyte subpopulation frequencies identified using FlowSOM clustering on d0 and 7 after vaccination as proportions of total DCs or total monocytes (n = 214). Horizontal lines indicate the median. Measured values of individual study participants are indicated by blue-colored dots and *P* values shown in the graphs (Wilcoxon test, Bonferroni corrected).

As the virus is present in the blood with a peak between days 3 to 7 after vaccination (44), direct contact between the virus and APCs could induce the observed ISG response. DCs can be infected and respond to direct contact with the YF17D virus through the activation of diverse pattern-recognition receptors, triggering cellular activation and cytokine secretion, including IFN-α (47–51). However, expression of IFN transcripts in the various APC subsets in peripheral blood was minimal or undetectable (in the case of IFN-α) by bulk and scRNA-seq, in the individuals and time points used for this study. In line with our findings, Hou et al. failed to detect IFN-α/-β/-λ mRNA expression in PBMC at earlier time points (4 and 24 h) in a cohort of 21 vaccinees (6). Additionally, our scRNA-seq data revealed a synchronized shift of the majority of cells within DC and monocyte subpopulations toward ISG-expressing clusters after vaccination consistent with a response to IFNs produced at the vaccination site or other tissues containing the vaccine virus and released into the circulation. However, neither IFN-α/-β nor IFN-γ or IFN-λ could be detected in plasma samples of our cohort using a sensitive bead-based multiplex assay. But even in acute flares of systemic lupus erythematosus with high ISG expression in PBMCs IFNs are only detectable in the plasma using ultrasensitive methods (52) suggesting that IFNs could be present in the blood of our vaccinees at very low concentrations. In fact, we observed in our bulk transcriptome analysis that also B cells upregulated ISGs on day 7 after vaccination reflecting a more general innate immune activation state induced by IFNs in circulating immune cells at this time point. We observed a higher expression of type I IFN module genes compared to type II IFN module genes in blood DCs and monocytes suggesting that type I IFNs are the dominant cytokines inducing the ISG response, but IFN-γ produced early after YF17D vaccination by NK cells (53, 54) may also contribute. It was described for SARS-CoV-2 mRNA vaccination for example that the frequency of myeloid cells with increased ISG expression emerging shortly after booster vaccination correlated with plasma IFN-γ levels at this time point (55).

SIGLEC1/CD169 expression is induced by IFN-α, IFN-β, and IFN-ω, but not IFN-γ (56) suggesting a role especially in antiviral defense (57) and as a marker of acute viral infection (30, 58, 59). We identified SIGLEC1 upregulation as a sensitive indicator of the early systemic response to IFNs and the transient activation state elicited in blood cDCs and monocytes by YF17D vaccination, which correlated with plasma CXCL10 levels and early antibody responses. A transient induction of SIGLEC1/CD169 expression on monocytes and CD1c$^+$ DCs associated with the IFN response signature was also reported after booster vaccination with a VSV-vectored HIV-1 vaccine (60). In our study, simultaneous upregulation of SIGLEC1 and costimulatory molecules indicated a temporary IFN-mediated functional maturation of cDCs as a characteristic feature of YF17D vaccination that may promote induction of adaptive immunity. We found an association of high SIGLEC1 upregulation on day 7 with high neutralizing antibody titers and virus-specific IgM titers on day 14 after vaccination providing a link between the systemic IFN response and rapid production of high titers of protective antibodies. Our findings resonate with an Ebola vaccine study that demonstrated upregulation of ISGs by the rVSVΔG-ZEBOV-GP vaccine and correlation with subsequent protective antibody titers (61). The type I IFN response may be directly linked to rapid antibody induction via activity of type I IFN on B cells promoting differentiation into antibody-secreting cells (62–64). In addition, type I IFN induces in DCs, monocytes, and neutrophils the secretion of B cell activating factor (BAFF), a critical survival factor for B cells, thereby supporting the neutralizing antibody response to infection (64, 65). Furthermore, IFN-induced activation of APCs supports B cell differentiation in germinal centers and antibody response via induction of T follicular helper cells (66), which we found to be rapidly activated within the first week after YF17D vaccination correlating with neutralizing

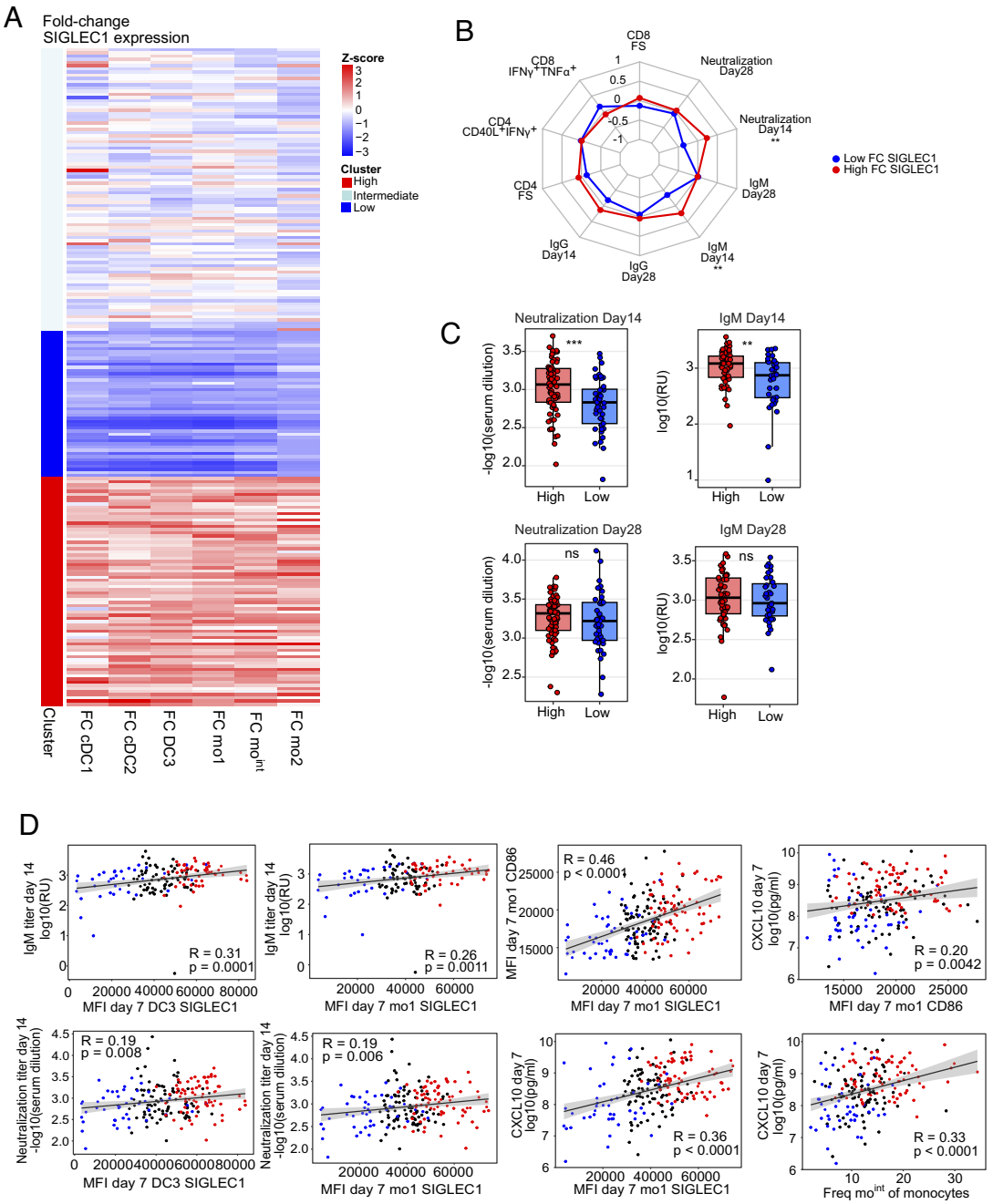

Fig. 7. SIGLEC1 upregulation is associated with the early protective antibody response to YF17D. (*A*) Unsupervised hybrid hierarchical k-means clustering performed on the scaled fold-changes between day 7 and baseline in the expression of SIGLEC1 for DC and monocyte populations. (*B*) A radar plot illustrating the association of vaccination endpoints for the two clusters identified in *A*, denoting high SIGLEC1 upregulation in red and low in blue. Vaccination endpoints include antigen-specific CD4 and CD8 functional scores (FS), the frequency of antigen-specific CD40L$^+$ IFN-γ$^+$ CD4$^+$ T cells, the frequency of antigen-specific IFN-γ$^+$ TNF-α$^+$ CD8$^+$ T cells and the yellow fever-specific IgG, IgM, and neutralizing antibody titers on day 14 and day 28 postvaccination. The data were scaled, and the radar plot depicts the means, with significance estimated using a Student's *t* test. (*C*) Boxplots comparing the neutralization and IgM antibody titers on days 14 and 28 for individuals with high or low SIGLEC1 upregulation identified in *A*. Significance was calculated using a Wilcoxon rank-sum test. (*D*) Spearman correlation analysis was conducted between the indicated parameters. Correlation coefficients, *P*-values, and linear regression lines are shown for all individuals and for those with high (red) and low (blue) SIGLEC1 upregulation identified in *A*. Statistical significance is depicted as follows: $*P \le 0.05$, $**P \le 0.01$, and $***P \le 0.001$ for (*B* and *C*).

antibody titers (12). Gressier et al. showed that conditioning of murine DCs with type I IFNs increased responsiveness to CD40 engagement by CD40L expressed on T helper cells leading to optimal priming of CD8$^+$ T cells (67). However, we did not find a positive correlation of SIGLEC1 expression in DCs or monocytes with the frequency of YF17D-specific CD8$^+$ T cells on day 28 nor the neutralizing antibody titers at that time point after YF17D vaccination suggesting that the early positive effect of APC activation may be counteracted by other mechanisms. For example, IFN-mediated reduction of viral replication may limit the availability of viral antigen for B cell activation and for CD8$^+$ T cell induction, which was shown to be determined by the YF17D viral load (44).

While all blood APC populations exhibited upregulation of a common set of ISGs and activation markers on day 7 postvaccination, distinct subset-specific responses to YF17D vaccination were evident underscoring the diverse and specialized functions of APC subpopulations in response to vaccination. pDCs for example did not significantly upregulate SIGLEC1 but other ISGs suggesting a differential response to IFNs and acquisition of a different activation

state than cDCs and monocytes. The specific upregulation of LAMP3 in cDC1 may indicate preferential conversion of this cell type to a mature migratory DC type which has been described in tumors and inflamed tissues (68, 69). Monocytes and DC3 showed heightened expression of various chemokines, including CXCL10, CCL7, and CCL2, aligning with their proinflammatory potential (29). The similar transcriptomic responses of cDC2, DC3, and monocytes after vaccination with YF17D are consistent with the reported convergence of transcriptomic changes in DC3, monocytes, and cDC2 following type I IFN stimulation demonstrating their close relationship and distinction from other APC subtypes (70). We also noticed that gene sets involved in translation, ribosome biogenesis, and oxidative phosphorylation were underrepresented in classical monocytes and pDCs after vaccination but enriched in intermediate monocytes and cDC subsets indicating differences between cell types in the metabolic response to vaccination. A decrease in oxidative phosphorylation and switch to glycolysis is associated with a proinflammatory response of monocytes to microbial stimulation and an innate immune training effect after exposure to beta-glucan or the BCG vaccine (71). For pDCs it was shown that type I IFN increases oxidative phosphorylation and fatty acid oxidation required for pDC activation in response to TLR stimulation (72). Thus, further investigation of changes in metabolism of monocyte and DC subpopulations after viral vaccination and the relevance for vaccine responses is warranted.

In conclusion, our study presents a comprehensive analysis of the transcriptomic responses of blood APC subpopulations to YF17D vaccination, highlighting a global ISG response within and across diverse subsets as well as cell type-specific responses. Notably, we found that upregulation of SIGLEC1 expression which represents IFN-induced activation in blood cDCs and monocytes is associated with early but not later protective antibody titers, unveiling a pivotal link between IFN-mediated APC activation and early humoral immunity. Thus, our study provides insights and resources to inform development of vaccines to rapidly induce protective immunity in naïve individuals.

Material and Methods

See *SI Appendix*, *Extended Methods* for more details.

Sample Collection and Study Design. The yellow fever vaccination study was conducted by the Department of Clinical Pharmacology of the University Hospital, LMU Munich, Germany. The study protocol was approved by the Institutional Review Board of the Medical Faculty of LMU Munich (IRB #86-16) and adhered to the most recent version of the Declaration of Helsinki (registered as ISRCTN17974967). All participants were healthy (aged 19 to 44 y, *SI Appendix*, Table S1) and had not been previously exposed to wild-type YFV, and were not previously immunized against YF. After giving informed consent, the patients received a single subcutaneous injection of the YF17D vaccine (Stamaril, Sanofi Pasteur, Lyon, France) at the Division of Infectious Diseases and Tropical Medicine at LMU Munich. Blood was drawn directly before vaccination and on days 3, 7, 14, and 28 after vaccination. PBMC were isolated by Ficoll density gradient centrifugation and frozen.

Flow Cytometric Analysis and Cell Sorting. Cryopreserved PBMC samples of vaccinees containing 1.5 to 3 × 10^6 cells were thawed, processed, stained, and analyzed by flow cytometry in four batches. The exploratory batch of 10 donors included time points days 0, 3, 7, and 14. The follow-up cohort of 214 patients included only day 0 and day 7 after vaccination and was separated into three batches measured within 1 wk of 60, 82, and 78 vaccinees each. Analysis of flow cytometric data was performed in Flow Jo, version 10.8.1. Living single cells in the HLA DR^+ Lin^- gate were exported from Flow Jo and used for further analysis in R. For sorting APC populations for bulk RNA sequencing analysis, T cells were separated via CD3 magnetic bead isolation, and the CD3 negative cell fraction was stained with antibody master mix, washed, and subsequently used for cell sorting on BD FACSAria Fusion (BD Biosciences).

Bulk RNA Sequencing Using SmartSeqv2. RNA was isolated from sorted cells using the Qiagen RNeasy Plus Microkit (Qiagen, Hilden, Germany). The Smart-Seqv2 protocol was performed with minor modifications. Samples were sequenced with NextSeq1000 using 100 bp paired-end sequencing. The number of reads was counted using HTSeq-count (0.6.1p1). Analysis was performed using DESeq2 (v1.34.0), fgsea, and ranked gene lists.

Single-Cell RNA Sequencing Using 10× Chromium. Gene expression libraries were prepared according to the manufacturer's protocol (10× Genomics). All libraries were sequenced using a NovaSeq 6000 (Illumina) to achieve 25,000 reads/cell for gene expression and 5,000 reads/cell for protein expression. Droplet libraries were processed using Cell Ranger v4.0. Reads were aligned to the GRCh38. Data were analyzed using Seurat and scVelo.

Quantification of Plasma Cytokines, Antibody Titers, and T Cell Responses. Cytokine concentrations were measured in plasma samples using Bio-Plex Multiplex Assay (Bio-Rad Laboratories, USA). The neutralizing antibody titers in serum samples were quantified by a Fluorescence Reduction Neutralization Test (FluoRNT) as previously described (73). YF17D-specific antibodies in human serum samples were quantified with an in-house ELISA using recombinantly produced soluble E protein or YF17D-virion as antigens as described (15, 74). These results have been published in a separate manuscript. To detect specific T cell responses PBMC were stimulated with live YF17D virus (1.5 × 10^7 PFU/mL) or with the equivalent volume of purified supernatant of uninfected cells (unstimulated control) for 20 h with addition of Brefeldin A (BioLegend) and anti-CD107a (clone H4A3, BD Biosciences) for the last 4 h followed by intracellular staining.

Statistical Analysis. Statistical analysis for scRNA seq data was performed as described above. Statistical analysis of flow cytometry data was performed in GraphPad Prism (v 9.1.0) or in R using ggpubr (v 0.5.0) Kruskal–Wallis test, or Wilcoxon test with Bonferroni correction as indicated in the individual figure legends. Vaccinees were clustered according to the fold-change in SIGLEC-1 expression in DCs and monocytes using hybrid hierarchical k-means clustering. Spearman rank correlation analysis was performed in R.

Data, Materials, and Software Availability. RNA-sequencing data are available at https://doi.org/10.5281/zenodo.13844224 (75). All other data are included in the manuscript and/or supporting information.

ACKNOWLEDGMENTS. We thank Yvonne Schäfer and Frank Dahlström for technical assistance. We also thank Arne Kroidl, Günter Fröschl, and Kristina Huber for serving as clinical study investigators. We acknowledge the Core Facility Flow Cytometry of the Biomedical Center, Ludwig-Maximilians-Universität München, and thank Lisa Richter and Pardis Khosravani. We acknowledge Eduardo Beltran for providing valuable advice. We also thank all the cohort participants who voluntarily participated in the study and donated samples. Parts of this work have been performed for the doctoral theses of E.W., A.S.-P., M.Z., T.E., and S.R. at the LMU Munich. This work was funded by the Deutsche Forschungsgemeinschaft (DFG) Project No. 210592381 SFB1054-TPA06 to A.B.K. and Project No. 369799452 TRR237-TPB14 to A.B.K. and S.R. The project received additional support from FlavImmunity a combined grant of the DFG Project No. 391217598 to S.R. and A.B.K. and the French National Research Agency (ANR) Project No. ANR-17-CE15-0031-01 to G.B.-S. The project has received additional funding from the European Union's Horizon Europe research and innovation programme under Grant Agreement No. 101137459–Yellow4FLAVI–"Deconstructing the protective immunity of yellow fever virus 17D to inform flavivirus vaccine design" to S.R., A.B.K., and G.B.-S. This work was additionally supported by grants of the iMed consortium of the German Helmholtz Societies and the Einheit für Klinische Pharmakologie, Helmholtz Zentrum München, Neuherberg, Germany, to S.R. E.W. received funding from the Friedrich–Baur–Stiftung and a scholarship from the Villigst Foundation.

Author affiliations: [a]Institute for Immunology, Biomedical Center, Faculty of Medicine, LMU, Munich D-82152, Germany; [b]Division of Clinical Pharmacology, University Hospital, Ludwig-Maximilans-Universität München, Munich D-80336, Germany; [c]Einheit für Klinische Pharmakologie Helmholtz Zentrum München, German Research Center for Environmental Health, Neuherberg D-85764, Germany; [d]Division of Infectious Diseases and Tropical Medicine, University Hospital, LMU, Munich D-80802, Germany; [e]Institut Pasteur, Université Paris Cité, CNRS UMR 3569, Unité de Virologie Structurale, Paris 75724, France; and [f]Core Facility Bioinformatics, Biomedical Center, Faculty of Medicine, LMU, Munich D-82152, Germany

1. S. A. Fuertes Marraco *et al.*, Long-lasting stem cell-like memory CD8+ T cells with a naïve-like profile upon yellow fever vaccination. *Sci. Transl. Med.* **7**, 282ra248 (2015).
2. E. Gotuzzo, S. Yactayo, E. Córdova, Efficacy and duration of immunity after yellow fever vaccination: Systematic review on the need for a booster every 10 years. *Am. J. Trop. Med. Hyg.* **89**, 434–444 (2013).
3. K. Kling *et al.*, Duration of protection after vaccination against yellow fever: A systematic review and meta-analysis. *Clin. Infect. Dis.* **75**, 2266–2274 (2022).
4. J. D. Poland, C. H. Calisher, T. P. Monath, W. G. Downs, K. Murphy, Persistence of neutralizing antibody 30–35 years after immunization with 17D yellow fever vaccine. *Bull. World Health Organ.* **59**, 895–900 (1981).
5. D. Gaucher *et al.*, Yellow fever vaccine induces integrated multilineage and polyfunctional immune responses. *J. Exp. Med.* **205**, 3119–3131 (2008).
6. J. Hou *et al.*, A systems vaccinology approach reveals temporal transcriptomic changes of immune responses to the yellow fever 17D vaccine. *J. Immunol.* **199**, 1476–1489 (2017).
7. T. D. Querec *et al.*, Systems biology approach predicts immunogenicity of the yellow fever vaccine in humans. *Nat. Immunol.* **10**, 116–125 (2009).
8. P. Bastard *et al.*, Auto-antibodies to type I IFNs can underlie adverse reactions to yellow fever live attenuated vaccine. *J. Exp. Med.* **218**, e20202486 (2021).
9. N. Hernandez *et al.*, Inherited IFNAR1 deficiency in otherwise healthy patients with adverse reaction to measles and yellow fever live vaccines. *J. Exp. Med.* **216**, 2057–2070 (2019).
10. E. Winheim *et al.*, Distinct and dynamic activation profiles of circulating dendritic cells and monocytes in mild COVID-19 and after yellow fever vaccination. *Eur. J. Immunol.* **53**, e2250090 (2023).
11. R. S. Akondy *et al.*, The yellow fever virus vaccine induces a broad and polyfunctional human memory CD8+ T cell response. *J. Immunol.* **183**, 7919–7930 (2009).
12. J. E. Huber *et al.*, Dynamic changes in circulating T follicular helper cell composition predict neutralising antibody responses after yellow fever vaccination. *Clin. Transl. Immunol.* **9**, e1129 (2020).
13. E. A. James *et al.*, Yellow fever vaccination elicits broad functional CD4+ T cell responses that recognize structural and nonstructural proteins. *J. Virol.* **87**, 12794–12804 (2013).
14. N. P. Lindsey *et al.*, Persistence of yellow fever virus-specific neutralizing antibodies after vaccination among US travellers. *J. Travel. Med.* **25**, tay108 (2018).
15. A. Santos-Peral *et al.*, Prior flavivirus immunity skews the yellow fever vaccine response to cross-reactive antibodies with potential to enhance dengue virus infection. *Nat. Commun.* **15**, 1696 (2024).
16. A. M. Watson, L. K. Lam, W. B. Klimstra, K. D. Ryman, The 17D–204 vaccine strain-induced protection against virulent yellow fever virus is mediated by humoral immunity and CD4+ but not CD8+ T cells *PLoS Pathog.* **12**, e1005786 (2016).
17. R. S. Akondy *et al.*, Origin and differentiation of human memory CD8 T cells after vaccination. *Nature* **552**, 362–367 (2017).
18. T. Hagan *et al.*, Transcriptional atlas of the human immune response to 13 vaccines reveals a common predictor of vaccine-induced antibody responses. *Nat. Immunol.* **23**, 1788–1798 (2022).
19. S. Li *et al.*, Molecular signatures of antibody responses derived from a systems biology study of five human vaccines. *Nat. Immunol.* **15**, 195–204 (2014).
20. G. Fingerle *et al.*, The novel subset of CD14+/CD16+ blood monocytes is expanded in sepsis patients. *Blood* **82**, 3170–3176 (1993).
21. M. Kwissa *et al.*, Dengue virus infection induces expansion of a CD14(+)CD16(+) monocyte population that stimulates plasmablast differentiation. *Cell Host Microbe* **16**, 115–127 (2014).
22. D. Michlmayr, P. Andrade, K. Gonzalez, A. Balmaseda, E. Harris, CD14(+)CD16(+) monocytes are the main target of Zika virus infection in peripheral blood mononuclear cells in a paediatric study in Nicaragua. *Nat. Microbiol.* **2**, 1462–1470 (2017).
23. M. A. Martins *et al.*, Innate immunity phenotypic features point toward simultaneous raise of activation and modulation events following 17DD live attenuated yellow fever first-time vaccination. *Vaccine* **26**, 1173–1184 (2008).
24. P. See *et al.*, Mapping the human DC lineage through the integration of high-dimensional techniques. *Science* **356**, eaag3009 (2017).
25. E. Segura, Human dendritic cell subsets: An updated view of their ontogeny and functional specialization. *Eur. J. Immunol.* **52**, 1759–1767 (2022).
26. A. C. Villani *et al.*, Single-cell RNA-seq reveals new types of human blood dendritic cells, monocytes, and progenitors. *Science* **356**, eaah4573 (2017).
27. P. Bourdely *et al.*, Transcriptional and functional analysis of CD1c(+) human dendritic cells identifies a CD163(+) subset priming CD8(+)CD103(+) T cells. *Immunity* **53**, 335–352.e338 (2020).
28. U. Cytlak *et al.*, Differential IRF8 transcription factor requirement defines two pathways of dendritic cell development in humans. *Immunity* **53**, 353–370.e358 (2020).
29. C. A. Dutertre *et al.*, Single-cell analysis of human mononuclear phagocytes reveals subset-defining markers and identifies circulating inflammatory dendritic cells. *Immunity* **51**, 573–589.e578 (2019).
30. E. Winheim *et al.*, Impaired function and delayed regeneration of dendritic cells in COVID-19. *PLoS Pathog.* **17**, e1009742 (2021).
31. M. Alcántara-Hernández *et al.*, High-dimensional phenotypic mapping of human dendritic cells reveals interindividual variation and tissue specialization. *Immunity* **47**, 1037–1050.e1036 (2017).
32. F. B. Sulczewski *et al.*, Transitional dendritic cells are distinct from conventional DC2 precursors and mediate proinflammatory antiviral responses. *Nat. Immunol.* **24**, 1265–1280 (2023).
33. B. de Saint-Vis *et al.*, A novel lysosome-associated membrane glycoprotein, DC-LAMP, induced upon DC maturation, is transiently expressed in MHC class II compartment. *Immunity* **9**, 325–336 (1998).
34. P. F. Rodrigues *et al.*, pDC-like cells are pre-DC2 and require KLF4 to control homeostatic CD4 T cells. *Sci. Immunol.* **8**, eadd4132 (2023).
35. R. Edahiro *et al.*, Single-cell analyses and host genetics highlight the role of innate immune cells in COVID-19 severity. *Nat. Genet.* **55**, 753–767 (2023).
36. D. C. Busse *et al.*, Interferon-induced protein 44 and interferon-induced protein 44-like restrict replication of respiratory syncytial virus. *J. Virol.* **94**, e00297-20 (2020).
37. T. Kimura *et al.*, Ifit1 inhibits Japanese encephalitis virus replication through binding to 5′ capped 2′-O unmethylated RNA. *J. Virol.* **87**, 9997–10003 (2013).
38. J. W. Schoggins *et al.*, A diverse range of gene products are effectors of the type I interferon antiviral response. *Nature* **472**, 481–485 (2011).
39. T. S. Teng *et al.*, Viperin restricts chikungunya virus replication and pathology. *J. Clin. Invest.* **122**, 4447–4460 (2012).
40. F. Terenzi, D. J. Hui, W. C. Merrick, G. C. Sen, Distinct induction patterns and functions of two closely related interferon-inducible human genes, ISG54 and ISG56. *J. Biol. Chem.* **281**, 34064–34071 (2006).
41. F. Wrensch *et al.*, Interferon-induced transmembrane protein-mediated inhibition of host cell entry of ebolaviruses. *J. Infect Dis.* **212**, S210–S218 (2015).
42. L. Ghita *et al.*, Global and cell type-specific immunological hallmarks of severe dengue progression identified via a systems immunology approach. *Nat. Immunol.* **24**, 2150–2163 (2023).
43. X. Sun *et al.*, Transcriptional changes during naturally acquired Zika virus infection render dendritic cells highly conducive to viral replication. *Cell Rep.* **21**, 3471–3482 (2017).
44. R. S. Akondy *et al.*, Initial viral load determines the magnitude of the human CD8 T cell response to yellow fever vaccination. *Proc. Natl. Acad. Sci. U.S.A.* **112**, 3050–3055 (2015).
45. L. A. Camacho *et al.*, Immunogenicity of WHO-17D and Brazilian 17DD yellow fever vaccines: A randomized trial. *Rev. Saude Publica* **38**, 671–678 (2004).
46. S. Edupuganti *et al.*, A randomized, double-blind, controlled trial of the 17D yellow fever virus vaccine given in combination with immune globulin or placebo: Comparative viremia and immunogenicity. *Am. J. Trop Med. Hyg.* **88**, 172–177 (2013).
47. G. Barba-Spaeth, R. S. Longman, M. L. Albert, C. M. Rice, Live attenuated yellow fever 17D infects human DCs and allows for presentation of endogenous and recombinant T cell epitopes. *J. Exp. Med.* **202**, 1179–1184 (2005).
48. D. Bruni *et al.*, Viral entry route determines how human plasmacytoid dendritic cells produce type I interferons. *Sci. Signal.* **8**, ra25 (2015).
49. Y. Cong *et al.*, Characterization of yellow fever virus infection of human and non-human primate antigen presenting cells and their interaction with CD4+ T cells. *PLoS Negl. Trop. Dis.* **10**, e0004709 (2016).
50. F. Douam *et al.*, Single-cell tracking of flavivirus RNA uncovers species-specific interactions with the immune system dictating disease outcome. *Nat. Commun.* **8**, 14781 (2017).
51. T. Querec *et al.*, Yellow fever vaccine YF-17D activates multiple dendritic cell subsets via TLR2, 7, 8, and 9 to stimulate polyvalent immunity. *J. Exp. Med.* **203**, 413–424 (2006).
52. A. Mathian *et al.*, Monitoring disease activity in systemic lupus erythematosus with single-molecule array digital enzyme-linked immunosorbent assay quantification of serum interferon-α. *Arthritis Rheumatol.* **71**, 756–765 (2019).
53. P. C. Neves, D. C. Matos, R. Marcovistz, R. Galler, TLR expression and NK cell activation after human yellow fever vaccination. *Vaccine* **27**, 5543–5549 (2009).
54. P. C. Neves, J. R. Santos, L. N. Tubarão, M. C. Bonaldo, R. Galler, Early IFN-gamma production after YF 17D vaccine virus immunization in mice and its association with adaptive immune responses. *PLoS ONE* **8**, e81953 (2013).
55. P. S. Arunachalam *et al.*, Systems vaccinology of the BNT162b2 mRNA vaccine in humans. *Nature* **596**, 410–416 (2021).
56. P. Bourgoin, G. Biéchelé, I. Ait Belkacem, P. E. Morange, F. Malergue, Role of the interferons in CD64 and CD169 expressions in whole blood: Relevance in the balance between viral- or bacterial-oriented immune responses. *Immun. Inflamm. Dis.* **8**, 106–123 (2020).
57. S. Herzog, P. C. Fragkou, B. M. Arneth, S. Mkhlof, C. Skevaki, Myeloid CD169/Siglec1: An immunoregulatory biomarker in viral disease. *Front. Med. (Lausanne)* **9**, 979373 (2022).
58. A. S. Bedin *et al.*, Monocyte CD169 expression as a biomarker in the early diagnosis of coronavirus disease 2019. *J. Infect. Dis.* **223**, 562–567 (2021).
59. N. Sakumura *et al.*, CD169 expression on monocytes as a marker for assessing type I interferon status in pediatric inflammatory diseases. *Clin. Immunol.* **250**, 109329 (2023).
60. Y. Hao *et al.*, Integrated analysis of multimodal single-cell data. *Cell* **184**, 3573–3587.e3529 (2021).
61. E. Vianello *et al.*, Transcriptomic signatures induced by the Ebola virus vaccine rVSVΔG-ZEBOV-GP in adult cohorts in Europe, Africa, and North America: A molecular biomarker study. *Lancet Microbe* **3**, e113–e123 (2022).
62. G. Jego *et al.*, Plasmacytoid dendritic cells induce plasma cell differentiation through type I interferon and interleukin 6. *Immunity* **19**, 225–234 (2003).
63. C. L. Swanson *et al.*, Type I IFN enhances follicular B cell contribution to the T cell-independent antibody response. *J. Exp. Med.* **207**, 1485–1500 (2010).
64. N. Baumgarth, The shaping of a B cell pool maximally responsive to infections. *Annu. Rev. Immunol.* **39**, 103–129 (2021).
65. D. Giordano *et al.*, BAFF produced by neutrophils and dendritic cells is regulated differently and has distinct roles in antibody responses and protective immunity against West Nile Virus. *J. Immunol.* **204**, 1508–1520 (2020).
66. M. W. Dahlgren *et al.*, Type I interferons promote germinal centers through B cell intrinsic signaling and dendritic cell dependent Th1 and Tfh cell lineages. *Front. Immunol.* **13**, 932388 (2022).
67. E. Gressier *et al.*, CD4(+) T cell calibration of antigen-presenting cells optimizes antiviral CD8(+) T cell immunity. *Nat. Immunol.* **24**, 979–990 (2023).
68. S. Nakamizo *et al.*, Single-cell analysis of human skin identifies CD14+ type 3 dendritic cells co-producing IL1B and IL23A in psoriasis. *J. Exp. Med.* **218**, e20202345 (2021).
69. Q. Zhang *et al.*, Landscape and dynamics of single immune cells in hepatocellular carcinoma. *Cell* **179**, 829–845.e820 (2019).
70. M. Girard, J. C. Law, M. I. Edilova, T. H. Watts, Type I interferons drive the maturation of human DC3s with a distinct costimulatory profile characterized by high GITRL. *Sci. Immunol.* **5**, eabe0347 (2020).
71. R. J. W. Arts *et al.*, Immunometabolic pathways in BCG-induced trained immunity. *Cell Rep.* **17**, 2562–2571 (2016).
72. D. Wu *et al.*, Type 1 interferons induce changes in core metabolism that are critical for immune function. *Immunity* **44**, 1325–1336 (2016).
73. M. K. Scheck *et al.*, FluoRNT: A robust, efficient assay for the detection of neutralising antibodies against yellow fever virus 17D. *PLoS ONE* **17**, e0262149 (2022).
74. A. Santos-Peral *et al.*, Basal T cell activation predicts yellow fever vaccine response independently of cytomegalovirus infection and sex-related immune variations. *Cell Rep. Med.* **6**, 101946 (2025).
75. E. Winheim, A. Krug, Data from "Interferon-induced activation of dendritic cells and monocytes by yellow fever vaccination correlates with early antibody responses." Zenodo. https://doi.org/10.5281/zenodo.13844224. Deposited 26 September 2024.